A Numerical Study of Concrete Composite Circular Columns encased with GFRP I-Section using the Finite Element Method

Abbas Allawi

Department of Civil Engineering, College of Engineering, University of Baghdad, Baghdad, Iraq
a.allawi@uobaghdad.edu.iq

Hiba Shihab Ahmed

Department of Civil Engineering, College of Engineering, University of Baghdad, Baghdad, Iraq
Heba.Ahmed2201M@coeng.uobaghdad.edu.iq (corresponding author)

Riyadh Hindi

Department of Civil Engineering, Saint Louis University, St. Louis, USA
riyadh.hindi@slu.edu

ABSTRACT

This paper presents ABAQUS simulations of fully encased composite columns, aiming to examine the behavior of a composite column system under different load conditions, namely concentric, eccentric with 25 mm eccentricity, and flexural loading. The numerical results are validated with the experimental results obtained for columns subjected to static loads. A new loading condition with a 50 mm eccentricity is simulated to obtain additional data points for constructing the interaction diagram of load-moment curves, in an attempt to investigate the load-moment behavior for a reference column with a steel I-section and a column with a GFRP I-section. The result comparison shows that the experimental data align closely with the simulation results regarding the ultimate strength, deformation, and failure modes, thereby validating the accuracy of the considered models. On the other hand, the numerical results of the column specimens under 50 mm eccentric load demonstrated that, in that case, the ultimate load of the columns decreased. The capacity of the reference column, a column with steel I-section, and a column with GFRP I-section decreased to 67%, 63%, and 64%, respectively compared with the columns tested under concentric load. The analytical investigation predicted the load-carrying capacity and bending moment capacity of the specimens with good accuracy. Based on the experimental curves, and the high strength found in the specimens that use the steel I- and GFRP I-sections, a good agreement between the numerical simulation and the experimental results was noticed.

Keywords-composite column; GFRP I-section; steel I-section; finite element analysis; ABAQUS

I. INTRODUCTION

The Glass Fiber Reinforced Polymer (GFRP) profile is a collection of heavy-duty, corrosion-resistant fiberglass profiles suitable for a wide range of applications. Its ability to guard against deterioration from industrial chemicals and environmental factors makes it a logical and cost-effective alternative to steel [1-10]. This paper is a continuation of the experimental research conducted in [11], which presented an experimental program that examined the behavior of steel and GFRP-I-section encased concrete columns. The parameters that were examined were the amplitude of load eccentricity and the type of internal reinforcement. The concrete specimens tested under concentric, eccentric with 25 mm eccentricity, and flexural loading included the steel reinforced, steel I-section

encased, and GFRP I-section encased concrete columns. All the details of the reinforcing specimens, specimen dimensions, material properties, and the type of testing performed were analyzed in [11]. The current paper also presents a numerical model for the aforementioned specimens, which aims to validate the experimental findings using the ABAQUS software and to predict the load-interaction diagrams of circular concrete specimens encased in GFRP.

II. NUMERICAL PART

A. Modeling Parts, Material Properties, and Boundary Conditions

The geometrical modeling requires six parts in ABAQUS 2019 commercial version. These are the concrete column,

spiral transverse reinforcement, longitudinal reinforcing steel bar, I-section, and supporting plates or steel cups. It is worth noting that the generated parts are simulated in a three-dimensional (3D) space. All the aforementioned parts were built using 3D deformable components. To build the I-section, 2D deformable pieces were utilized. However, the 1D wire technique was deployed to simulate longitudinal bars in steel reinforcement models, which resulted in one-dimensional components. This investigation modeled concrete, spiral reinforcement, steel loading caps, and steel saddle plates using solid C3D8R elements with a 20 mm mesh size concrete column, 50 mm mesh size for spiral, and 25 mm for cups and steel saddle plates. The longitudinal steel bar was modeled deploying a T3D2 element with a 50 mm mesh size, and the steel and GFRP I-section were modeled utilizing S4R shell elements S4R with a 25 mm mesh size. A numerical example was created to determine the reliable mesh size. This site was chosen using suitable convergence criteria to closely match the experimental findings of Figure 1.
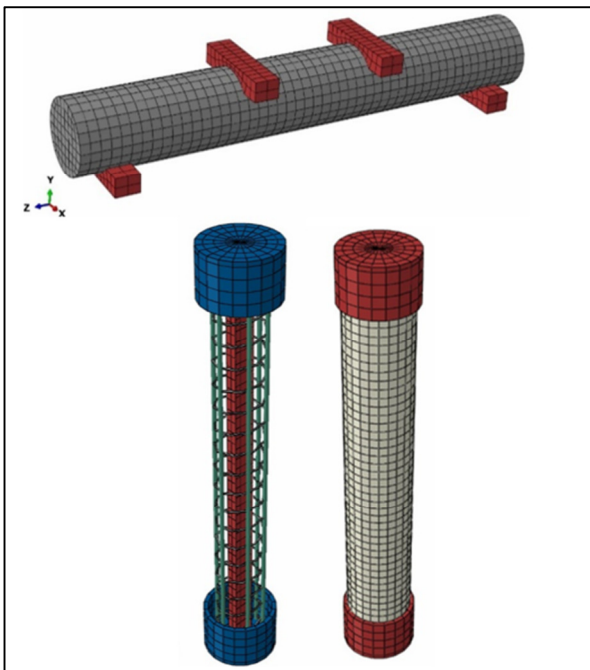

Fig. 1.   Specimen mesh.

The mechanical properties of the materials mentioned above and the concrete properties used in ABAQUS were thoroughly explained in [12]. Each column's base was restrained for any number of Degrees of Freedom (DoF) for all displacements, in x, y, and z directions, while allowing rotations around the x-axis. The top end of each column stayed unrestrained in the y direction, while an equally distributed axial force was delivered employing the displacement control approach observed in Figure 2. For the specimens which were tested under flexural load, one support, the pinned support, was restrained for all displacements in x, y, and z directions. The second support and the roller support, only restrained displacements in the x and y direction, as shown in Figure 2.
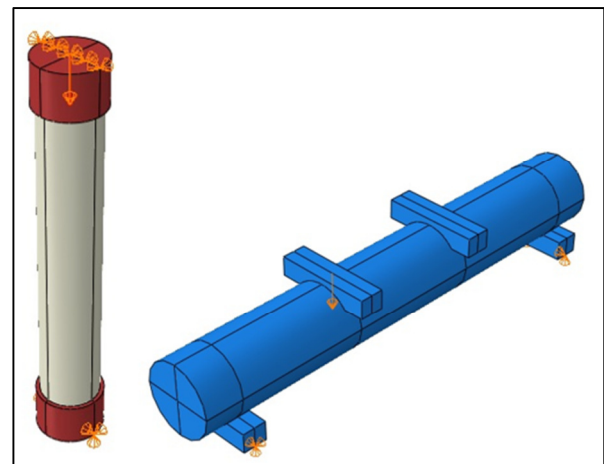

Fig. 2.   Boundary conditions and applied load.

B. Material Properties and Modeling

Defining the property, meaning the property of the material, is an important step in the Finite Element Method (FEM). The section composite columns are made of concrete, steel longitudinal and spiral reinforcement, and steel I-section or GFRP I-section. All the material properties used for the analysis are presented in Table I.

TABLE I.   MATERIALS PROPERTIES

No.	Material	Density (t/mm³)	Young modulus (MPa)	Poisson's ratio
1.	Normal strength concrete	2.4×10^{-9}	32920.6	0.2
2.	Longitudinal steel bar 6 mm	7.8×10^{-9}	210000	0.3
3.	Transfer steel bar 4 mm	7.8×10^{-9}	210000	0.3
4.	Steel I-section	7.8×10^{-9}	210000	0.3
5.	GFRP I-section	1.85×10^{-9}	40410	0.33

The nonlinear behavior of concrete was considered using the concrete-damaged plasticity CDP model in the software. The CDP model depicts the mechanisms of crushing and cracking failure that occur in concrete. The stress-strain relationship predicted in [12] was deployed to simulate the behavior of concrete in compression. Authors in [13] proposed the constitutive stress-strain relation for concrete under tension. Perfect plastic can be employed to model the materials of the reinforcing steel bars. On the other hand, the steel I-section was modeled as a relationship adopted by [14]. In ABAQUS, the GFRP section used in specimens tested under concentric and eccentric loads was modeled utilizing the assumption of isotropic linear elastic behavior without having employed any damage criterion. On the other hand, to model the GFRP I-section in the specimen that was tested under flexural load, two stages of modeling were deployed: the elastic phase, and the material type "LAMINA", which was used to simulate the elastic behavior of GFRP sections [15]. The Hashin damage criteria failure model, which establishes the failure mode, is deployed to depict the second phase, namely the failure stage [16].

C. Finite Element Validation and Test Results

1) Load Capacity and Load-Deflection Curve of Numerical and Experimental Results

Regarding the finite element models, the observed percentage of variance for the load capacity and the corresponding deflection curve were found. These results were subsequently compared with the experimental results as can be seen in Tables II and III. According to the comparison results, a strong agreement between the finite element predictions and the experimental data was observed. The load-deformation curves for concentric loading, eccentric loading (25 mm), and flexural loading, illustrated in Figures 3-6 and Figures 7-8, respectively, were compared with the experimental curves attained from test results.

TABLE II.   LOAD CAPACITY OF NUMERICAL AND EXPERIMENTAL RESULTS

Specimens	Pu Exp(kN)	Pu FEM (kN)	P_u FEM/P_u Exp
R-E00	766.7	811.2	1.06
IS-E00	835.4	862.2	1.03
IG-E00	788.6	816	1.03
R-E25	421.4	438	1.04
IS-E25	471.5	486.2	1.03
IG-E25	462.4	471.2	1.02
R-F	35	38.9	1.11
IS-F	75	79	1.05
IG-F	47.8	51	1.06

TABLE III.   DISPLACEMENT OF NUMERICAL AND EXPERIMENT RESULTS

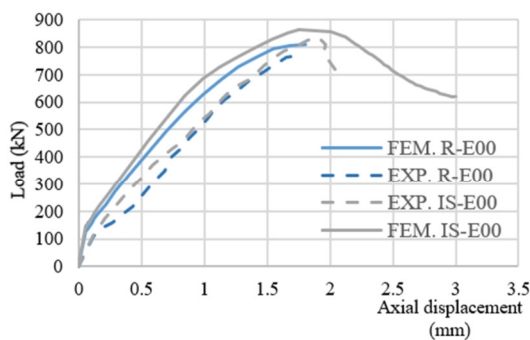| Specimens	Δu Exp.(mm)	Δu FEM (mm)	Δu FEM/ Δu Exp
R-E00	1.67	1.80	1.08
IS-E00	1.91	1.75	0.91
IG-E00	1.71	1.79	1.04
R-E25	3.61	2.91	0.8
IS-E25	3.23	3.65	1.13
IG-E25	3.77	3.41	0.9
R-F	5.96	4.86	0.82
IS-F	8.47	8.74	1.03
IG-F	11.86	8.34	0.7

Fig. 3.   Numerical validation of the IS-E00 and R-E00 specimens.
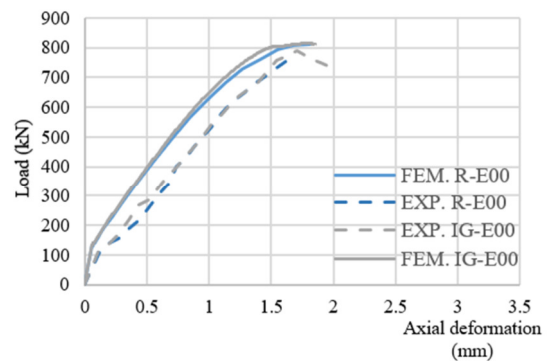

Fig. 4.   Numerical validation of the IG-E00 and R-E00 specimens.
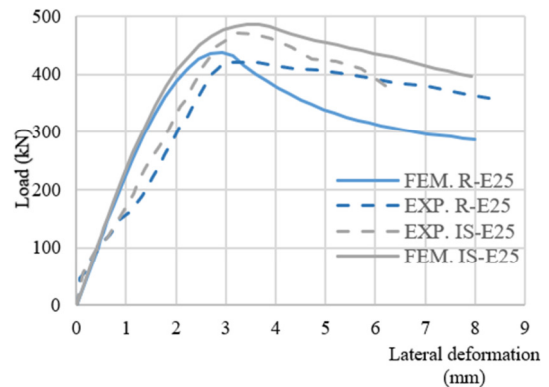

Fig. 5.   Numerical validation of the IS-E25 and R-E25 specimens.
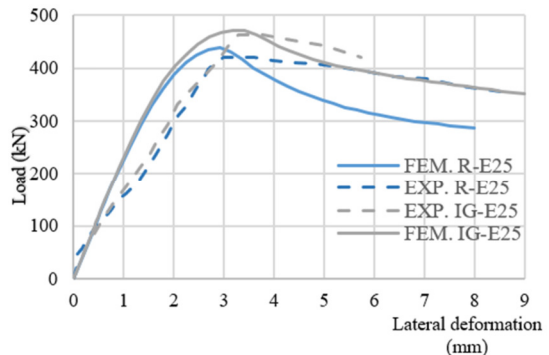

Fig. 6.   Numerical validation of the IG-E25 and R-E25 specimens.
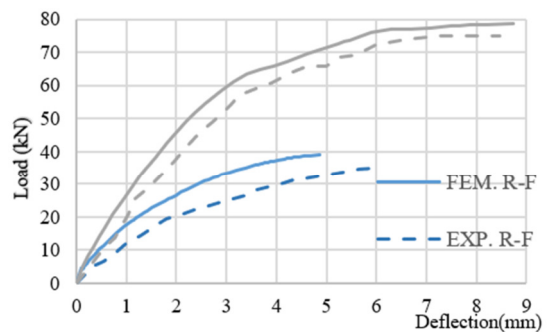

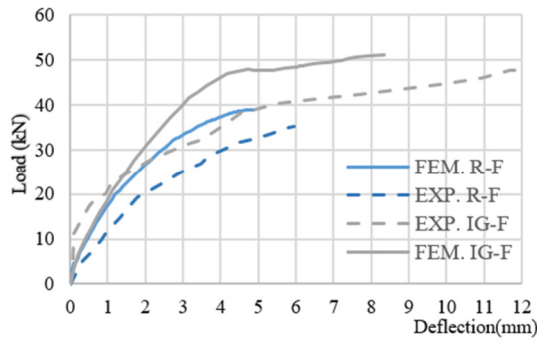Fig. 7.   Numerical validation of the IS-F and R-F specimens.

Fig. 8. Numerical validation of the IG-F and R-F specimens.

FEM accurately replicated the experimental findings, confirming its reliability. It should be noted that the numerical result curves were stiffer than those of the experimental work. In addition, there was a noticeable difference in the degradation rate between them.

2) Results of Column Simulation under 50 mm Eccentric load

A simulation modeling for the column specimens under eccentric load (50 mm), using FEM, is presented in this section. This simulation has been applied to the reference, column strengthened with I-section steel, and column strengthened with I-section GFRP to get extra points for drawing the interaction diagram of the load-moment curves. On the other hand, the results of this simulation indicate that when increasing the eccentricity to 50 mm, the ultimate load of columns decreases, while the capacity of R-E50, IS-E50, and IG-E50 decreases to 67%, 64%, and 63%, respectively, regarding the specimens tested under concentric load. Furthermore, the specimen IS-E50 achieved an ultimate load of 15.7%, which was greater than that of the R-E50 specimen. The IG-E50 specimen achieved an 11% ultimate load, which was greater than that of the R-E50 specimen, as shown in Figure 9.
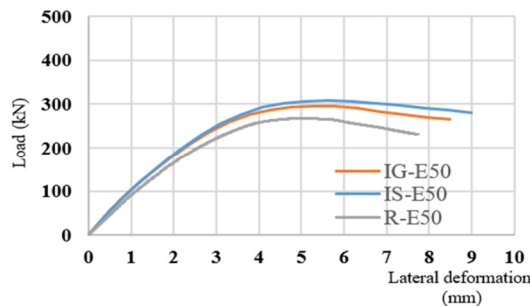

Fig. 9. Load-deformation curve of the specimens under eccentric load (50 mm).

3) Crack Pattern

The mode of failure was identified for every kind of specimen, with details being presented in [11], which showed matching results for the failure mode in the numerical analysis. The damage developed in each column is depicted in Figures 10(a), 10b, and 10c under flexural load, concentric load, and eccentric load (25 mm), respectively.
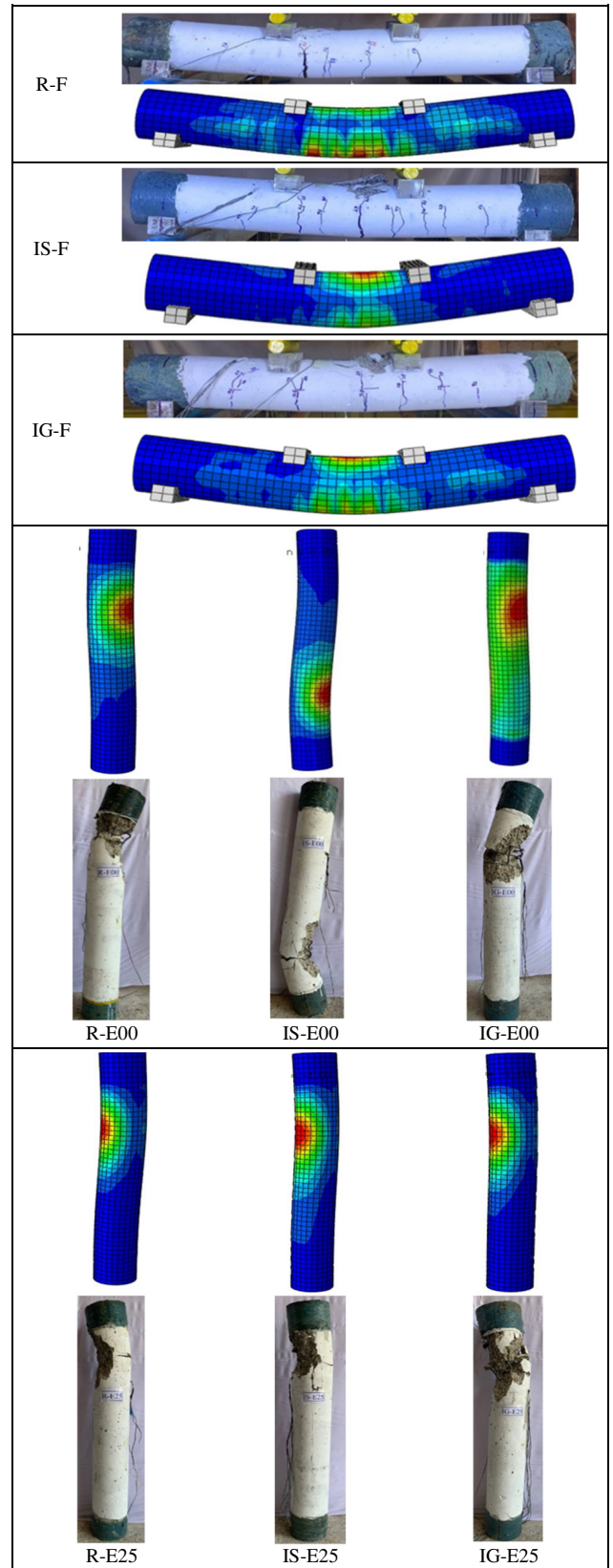

Fig. 10. (a) Specimens under flexural load, (b) specimens under concentric load, and (c) specimens under 25 mm eccentric load.

III.   THE INTERACTION DIAGRAM

Using four points, namely the concentric load (pure compression load), the 25 mm and 50 mm eccentricity load, and the flexural load (pure bending), the current study creates a numerical strength interaction diagram. The allowed bending moment and axial compression capacity of specimens are illustrated in this diagram. Equation (1) was used to determine the flexural moment at the column's mid-height under two compression eccentric loads, and (2) was utilized to compute the flexural moment when the specimen was tested as a beam:

$$M = P (e + \Delta) \qquad (1)$$

$$M = PL/6 \qquad (2)$$

where M is the bending moment, P is the maximum applied load, e is the eccentricity of the applied load, Δ is the lateral deformation at the maximum applied load, and L is the clear span of the beam. Table IV displays the experimental and numerical results of (1) and (2):

TABLE IV.   RESULTS OF EXPERIMENTAL AND NUMERICAL INTERACTION DIAGRAM PARAMETERS

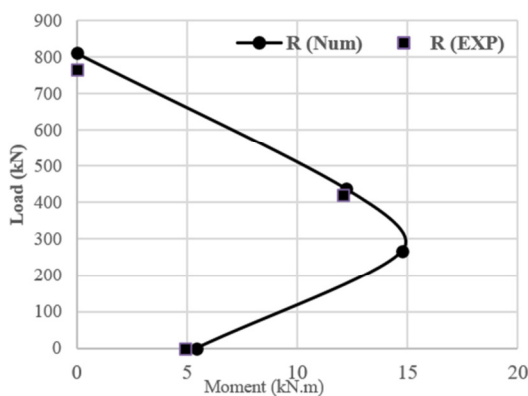| Specimen ID	Numerical results		Experimental results	
	M (kN.m) X axis	P (kN) Y-axis	M (kN.m) X-axis	P (kN) Y-axis
R-E00	0	811.2	0	766.7
R-E25	12.2	438	12.05	421.4
R-E50	14.76	267	—	—
R-F	5.44	0	4.9	0
IS-E00	0	862.2	0	835.4
IS-E25	13.92	486.2	13.31	471.5
IS-E50	17.18	309	—	—
IS-F	11.06	0	10.5	0
IG-E00	0	816	0	788.6
IG-E25	13.38	471.2	13.30	462.4
IG-E50	16.35	296	—	—
IG-F	7.14	0	6.69	0

Fig. 11.   Interaction diagrams of numerical and experimental strength for reference specimens.

The Figure curves and Table IV reveal that the specimens incorporating steel I-sections and GFRP I-sections exhibit high strength. Strengthening with I-sections significantly improves the column's performance under various loading conditions (concentric, eccentric with 25 mm eccentricity, and flexural) compared to the reference column without strengthening. This enhancement is attributed to the high efficiency of steel and

GFRP materials for structural strengthening. Additionally, a strong agreement was observed between the numerical simulations and experimental results. Figures 11-13 illustrate the load-moment interaction diagrams for the reference column, the column with a steel I-section, and the column with a GFRP I-section, respectively.
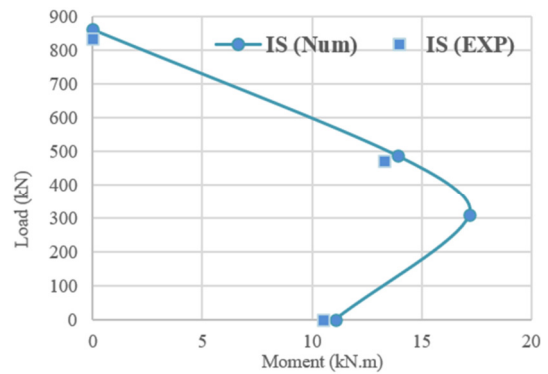

Fig. 12.   Interaction diagrams of numerical and experimental strength for a composite column with steel I-Section.
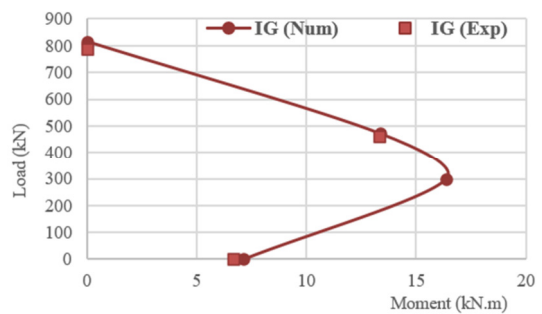

Fig. 13.   Interaction diagrams of numerical and experimental strength for a composite column with GFRP I-Section.

IV.   CONCLUSIONS

Based on the outcomes of this simulation study, the overall conclusions drawn are:

- The numerical results showed high agreement with the test findings for the ultimate strength, deformation, and failure modes demonstrated by the experimental data, which verified model accuracy.

- By using the Finite Element Method (FEM), the composite column achieved higher loading capacity using steel or GFRP I-section than the control columns for all loading conditions. That is, IS-E00 and IG-E00 achieved 6.3% and 1% higher than R-E00, respectively, while IS-E25 and IG-E25 obtained 11% and 7.6% more than R-E25, respectively. Also, the IS-F and IG-F specimens attained 103% and 31% more than the R-F, respectively.

- The numerical results of the column specimens under eccentric load (50 mm) demonstrated that when increasing the eccentricity to 50 mm, the ultimate load of columns decreased, in that the capacity of R-E50, IS-E50, and IG-

E50 decreased to 67%, 64%, and 63%, respectively compared with the columns tested under concentric load.

- A numerical investigation can predict the load-carrying capacity and bending moment capacity of the specimens. By creating a numerical interaction diagram, a good agreement between the numerical simulation and experimental results was noticed.

- According to the P-M diagram curves, high strength was observed in specimens utilizing steel I-section and GFRP I-section.

- The specimens IS-E50 and IG-E50 achieved higher ultimate load from the R-E50 specimen, namely 15.7% and 11%, respectively.

REFERENCES

[1] A. A. Allawi and S. I. Ali, "Flexural Behavior of Composite GFRP Pultruded I-Section Beams under Static and Impact Loading," *Civil Engineering Journal*, vol. 6, no. 11, pp. 2143–2158, Nov. 2020, https://doi.org/10.28991/cej-2020-03091608.

[2] T. H. Ibrahim and A. A. Allawi, "The Response of Reinforced Concrete Composite Beams Reinforced with Pultruded GFRP to Repeated Loads," *Journal of Engineering*, vol. 29, no. 01, pp. 158–174, Jan. 2023, https://doi.org/10.31026/j.eng.2023.01.10.

[3] E. M. Mahmood, A. A. Allawi, and A. El-Zohairy, "Flexural Performance of Encased Pultruded GFRP I-Beam with High Strength Concrete under Static Loading," *Materials*, vol. 15, no. 13, Jan. 2022, Art. no. 4519, https://doi.org/10.3390/ma15134519.

[4] T. H. Ibrahim, A. A. Allawi, and A. El-Zohairy, "Impact Behavior of Composite Reinforced Concrete Beams with Pultruded I-GFRP Beam," *Materials*, vol. 15, no. 2, Jan. 2022, Art. no. 441, https://doi.org/10.3390/ma15020441.

[5] E. M. Mahmood, A. A. Allawi, and A. El-Zohairy, "Analysis and Residual Behavior of Encased Pultruded GFRP I-Beam under Fire Loading," *Sustainability*, vol. 14, no. 20, Jan. 2022, Art. no. 13337, https://doi.org/10.3390/su142013337.

[6] E. M. Mahmood, T. H. Ibrahim, A. A. Allawi, and A. El-Zohairy, "Experimental and Numerical Behavior of Encased Pultruded GFRP Beams under Elevated and Ambient Temperatures," *Fire*, vol. 6, no. 5, May 2023, Art. no. 212, https://doi.org/10.3390/fire6050212.

[7] M. I. Ali, A. A. Allawi, and A. El-Zohairy, "Flexural Behavior of Pultruded GFRP–Concrete Composite Beams Strengthened with GFRP Stiffeners," *Fibers*, vol. 12, no. 1, Jan. 2024, Art. no. 7, https://doi.org/10.3390/fib12010007.

[8] T. H. Ibrahim, "Performance of Hybrid Rc Beams With Embedded Gfrp Section Under Static and Impact Loading," Ph.D. dissertation, University of Baghdad, Baghdad, Iraq, 2006.

[9] A. I. Said *et al.*, "Experimental and FE Investigations of Backfill Cover on Large-Diameter GRP Pipes," *CivilEng*, vol. 5, no. 3, pp. 646–672, Sep. 2024, https://doi.org/10.3390/civileng5030035.

[10] F. M. Bahlol and A. Al-Ahmed, "GFRP Encasing Efficiency on Enhancement Composite Beams under Static Loading," *Engineering, Technology & Applied Science Research*, vol. 14, no. 5, pp. 16897–16901, Oct. 2024, https://doi.org/10.48084/etasr.8064.

[11] H. S. Ahmed, A. Allawi, and R. Hindi, "Experimental Investigation of Composite Circular Encased GFRP I-Section Concrete Columns under Different Load Conditions," *Engineering, Technology & Applied Science Research*, vol. 14, no. 5, pp. 17286–17293, Oct. 2024, https://doi.org/10.48084/etasr.8521.

[12] A. A. Elwi and D. W. Murray, "A 3D Hypoelastic Concrete Constitutive Relationship," *Journal of the Engineering Mechanics Division*, vol. 105, no. 4, pp. 623–641, Aug. 1979, https://doi.org/10.1061/JMCEA3.0002510.

[13] D. A. Hordijk, *Local approach to fatigue of concrete*. W. D. Meimena b.v Delft, 1991.

[14] X. Yun and L. Gardner, "Stress-strain curves for hot-rolled steels," *Journal of Constructional Steel Research*, vol. 133, pp. 36–46, Jun. 2017, https://doi.org/10.1016/j.jcsr.2017.01.024.

[15] N. F. Hany, E. G. Hantouche, and M. H. Harajli, "Finite element modeling of FRP-confined concrete using modified concrete damaged plasticity," *Engineering Structures*, vol. 125, pp. 1–14, Oct. 2016, https://doi.org/10.1016/j.engstruct.2016.06.047.

[16] Z. Hashin, "Fatigue Failure Criteria for Unidirectional Fiber Composites," *Journal of Applied Mechanics*, vol. 48, no. 4, pp. 846–852, Dec. 1981, https://doi.org/10.1115/1.3157744.